

A Facile Synthesis of Cd Substituted Al Nano Chromites by Citrate Gel Method: A Comprehensive Study on Structural, Optical, Catalytic, Microbial and Anticancer Activities

Ch. Srikanth, P. Sailaja Kumari, R. Venkatesh Nayak, G. Vijaya Charan*

Department of Chemistry, University College of Science, Osmania University, Hyderabad, India

ABSTRACT

The current study gives the formation of cadmium (Cd) doped aluminum (Al) nano chromites by the citrate gel auto-combustion method. Structural, optical and biological activity of the synthesized chromites was performed. Microstructure and morphological analysis of the nano chromites were analyzed by X-ray diffraction (XRD), Field Emission Scanning Electron Microscopy, and Fourier-transform infrared (FTIR) studies. XRD confirms the single-phase cubic spinel structure of the Cd-Al nano chromites. The average crystalline size of the samples 19 nm to 25 nm calculated by Debye Scherrer equation from XRD pattern. FTIR spectrum confirms the metal-oxygen bonds around 400–600 cm⁻¹ wavenumber domain related to the spinel structure. Optical band gap energy ranges from 2.21 eV to 2.96 eV calculated by Tauc plots. Antibacterial activity of the materials performed four bacterial agents, namely, *Staphylococcus*, *Bacillus*, *Escherichia coli*, and *Klebsiella* by pour plate method. Hela cells were used to check the anticancer activity of the materials.

Key words: Aluminum-cadmium nanoparticles, Biological activity, Optical properties, X-ray diffraction studies.

1. INTRODUCTION

Nanoscience is the study of structures and materials on the scale of nanometers (1–100 nm), where unique physical, chemical, and biological properties emerge due to the dominance of quantum effects and increased surface area-to-volume ratio [1]. Nanotechnology involves the design, synthesis, manipulation, and application of these nanoscale materials for specific purposes. Nanomaterials are advanced materials with dimensions at the nanoscale, offering unique properties that differ significantly from their bulk counterparts [2]. They can be broadly categorized into carbon-based materials (e.g., graphene and carbon nanotubes), metal and metal oxide nanoparticles (e.g., silver, titanium dioxide, zinc oxide), ceramic nanomaterials, polymeric nanomaterials, and nanocomposites [3-5]. Each type finds applications across industries, such as electronics, catalysis, medicine, and energy storage, due to their high surface area, tunable optical properties, and mechanical strength. Among these, nano chromites, spinel-structured nanomaterials (AB_2O_4), hold particular importance for their multifunctional properties. Nano chromites such as $NiCr_2O_4$ and $CuCr_2O_4$ exhibit excellent catalytic activity, magnetic properties, and thermal stability, making them suitable for applications in pollutant degradation, energy storage, sensors, and magnetic storage devices [6,7]. Their ability to exhibit mixed valency and reversible redox behavior enhances their role in energy and environmental applications, positioning nano chromites as key materials in sustainable and advanced technological developments.

Cadmium (Cd) doped aluminum (Al) nano chromites are a class of spinel-structured materials with the general formula AB_2O_4 . These compounds belong to the family of mixed-metal oxides where Cd and Al occupy specific lattice positions, forming a cubic spinel structure with unique physical and chemical properties. Spinel structure with the general formula AB_2O_4 , where A is typically a divalent cation Cd^{2+} and B is a trivalent

cation Al^{3+} . The structure consists of a cubic close-packed oxygen lattice with cations occupying interstitial tetrahedral and octahedral sites. In normal spinel's like $CdCr_2O_4$, Cd^{2+} ions predominantly occupy the tetrahedral sites, while Al^{3+} ions occupy the octahedral sites [8,9]. This arrangement ensures charge neutrality and structural stability.

Nanoparticles can be synthesized using various methods, each tailored to achieve specific properties and applications. Physical methods like laser ablation and physical vapor deposition are ideal for creating high-purity particles but often require sophisticated equipment. Chemical approaches, such as sol-gel processing [10], poly acrylamide method [11], microemulsion, solid state, co-precipitation, and hydrothermal methods [12], offer versatility in producing nanoparticles with controlled size and morphology. Among these, the citrate gel auto-combustion method stands out due to its simplicity, cost-effectiveness, and ability to produce highly pure, homogeneously sized nanoparticles [13]. This method involves the use of metal nitrates and citric acid to form a gel, which undergoes self-sustained combustion to yield fine particles. Particularly effective for synthesizing spinel-structured materials like nano chromites, this method ensures phase purity, uniformity, and scalability, making it invaluable for applications in catalysis, energy storage, and environmental remediation [14].

*Corresponding author:

G. Vijaya Charan

E-mail: drvijayacharan@gmail.com

ISSN NO: 2320-0898 (p); 2320-0928 (e)

DOI: 10.22607/IJACS.2025.1301002

Received: 04th January 2025;

Revised: 18th January 2025;

Accepted: 22th January 2025;

Published: 02th February 2025



In this current study, we discussed the synthesis of $\text{Al}_{1-x}\text{Cd}_x\text{Cr}_2\text{O}_4$ where $x = 0.00, 0.02, 0.04, 0.06, 0.08$, and 0.10 nano chromites by citrate gel auto combustion method. The prepared samples characterized by X-ray diffraction (XRD), Scanning Electron Microscopy (SEM), and Fourier-transform infrared (FTIR) for structural studies. In addition, their optical, photocatalytic, and biological activity were investigated.

2. EXPERIMENTAL STUDIES

2.1. Samples Preparation

The Cd-doped Al nano chromites were synthesized using the citrate gel auto-combustion method, a versatile and efficient technique for producing nanomaterials with controlled composition and morphology. The synthesis begins with the dissolution of stoichiometric amounts of Al nitrate, Cd nitrate, and chromium nitrates in deionized water to prepare a clear solution of metal ions. Citric acid is then added in a molar ratio adequate to act as a chelating agent and fuel. The citric acid forms stable complexes with the metal ions, ensuring uniform distribution. Ammonia solution is added dropwise to the mixture to adjust the pH to a range of 7–8. This pH range is critical for facilitating the chelation process and preventing the precipitation of metal hydroxides. The solution is heated on a hot plate at approximately 80–90°C under continuous stirring to evaporate the water. As the water content reduces, the solution becomes viscous and eventually transforms into a gel. The temperature is increased

to 150°C. In this step, the gel undergoes a spontaneous combustion reaction. This combustion is driven by the redox reaction between metal nitrates (oxidizers) and citric acid (fuel). The process produces a porous, fluffy, ash-like material containing the Cd-doped Al nano chromites. The as-synthesized material is calcined at 500°C for 4 h in a muffle furnace. Calcination removes residual organic matter, enhances crystallinity, and ensures phase purity. This step is crucial for achieving the desired structural and functional properties of the nano chromites. The calcinated samples were grinded again for about one hour to form fine powder, resultant samples were analyzed by different characterization techniques. The synthesis procedure was shown in Figure 1.

2.2. Experimental Methods

A Rigaku 600 X-ray diffractometer was used for the XRD investigation. The Carl Zeiss Ultra 55 model was used for SEM analysis, and the Oxford INCAxact model handled energy-dispersive X-ray analysis. The Fluoromax Plus Spectrometer was utilized for photoluminescence (PL) analysis, the Shimadzu FTIR 8400 Spectrometer for FTIR analysis, and the Shimadzu ultraviolet (UV)-3600 Spectrometer for ultraviolet visible-diffuse reflectance spectroscopy (UV-DRS) analysis.

2.3. Antibacterial Activity Procedure

Gram-positive and Gram-negative bacterial active cultures, nutrient and potato dextrose agar media, yeast peptone extract media, and

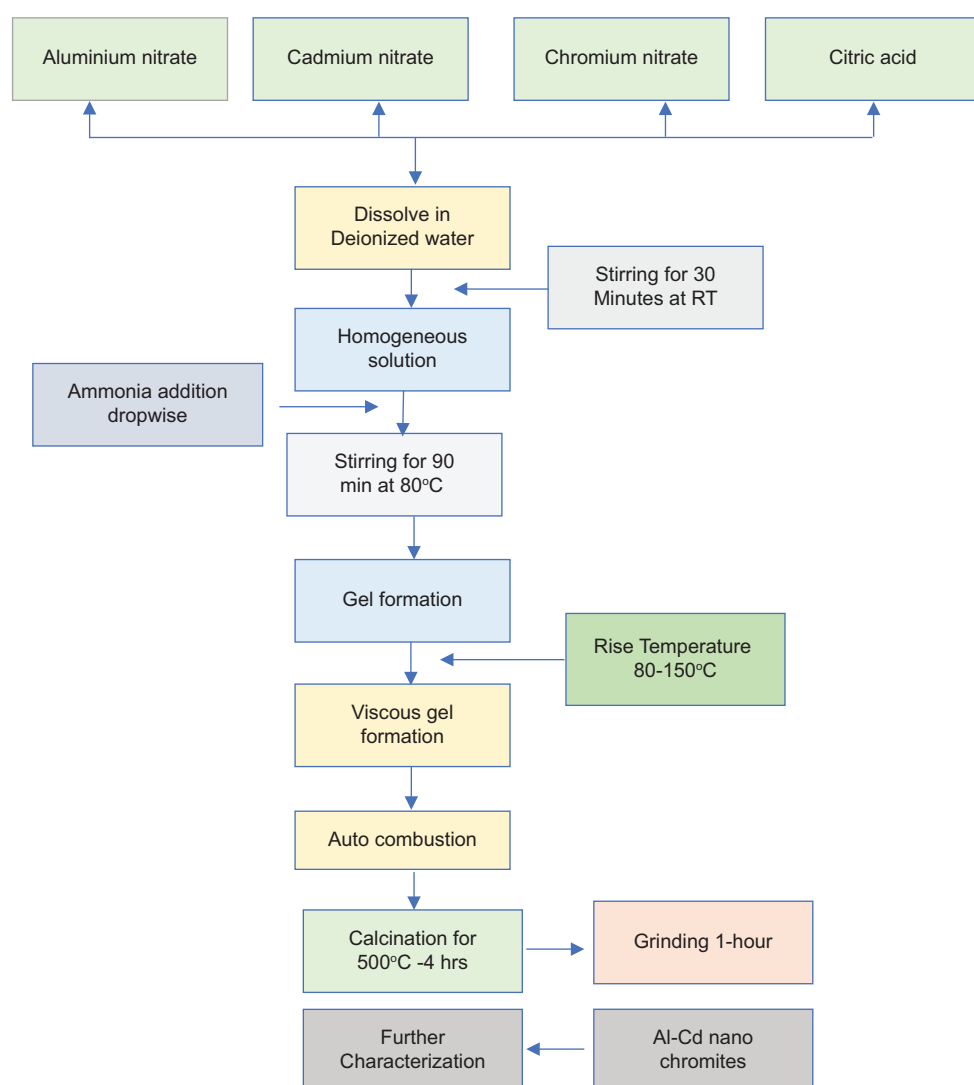


Figure 1: Flow chart of Citrate gel auto combustion method for preparation of aluminum-cadmium nanoparticles.

standard laboratory supplies. Petri plates, standard bacterial strain (Streptomycin -5 μ g/m), and bacterial incubator. After transferring the bacterial culture and 50 mL of nutritional media into a tiny conical flask, it is incubated for 8–12 h at 37°C. For the minimum inhibitory concentration assay, (or) minimum inhibitory concentration (MIC) assay, the produced chromite samples were created at various concentrations after being dissolved in 1 mL of dimethyl sulfoxide. Solvent was used to further dilute the produced MIC test liquid samples. The pour plate method was employed to conduct the antibacterial test. This entailed combining autoclaved agar medium just before it solidified with 1% of bacterial active culture, then transferring the combination into the plates. *Bacillus* and *Staphylococcus* were selected for Gram-positive bacteria in this case, whereas *Escherichia coli* and *Klebsiella* were selected for Gram-negative bacteria. After the plates had solidified, 100 μ L of material was added to each well, which had been made using a sterile well borer. These plates were incubated at 37°C for 18–24 h in a bacterial incubator. Each well of the plate was filled with 25 μ L, 50 μ L, 75 μ L, and 100 μ L increments of the samples that were evaluated for antibacterial activity. The contents were diluted with water or solvent until the volume reached 100 μ L. This made it possible to determine the samples' minimum inhibitory concentrations (MIC). In this experiment, samples containing 10 mg/mL were used, and appropriate dilutions were made.

2.4. Antifungal Activity Procedure

The antifungal activity of the synthesized samples was examined using *Aspergillus* and *Candida*. After autoclaving, a potato dextrose agar medium and yeast extract were made. Just before the media was poured onto the plates, an antibiotic (Streptomycin/Chloramphenicol) was added to stop bacterial contamination. Depending on the number of samples, sterile well borers were used to make 5mm wells after the plates had had time to set. A 100 μ L sample was put into each well. The plates were incubated at 25°C for 96 h before the results were recorded. To determine their minimum inhibitory concentrations (MIC), the antifungal activity-tested samples were placed into each well of the plate in increments of 25, 50, 75, and 100 μ L. Water or a dilution solvent was added to bring the level up to 100 μ L.

2.5. MTT Assay Method

Yellow 3-(4,5-dimethylthiazol-2yl)-2,5-diphenyl tetrazolium bromide reduction by mitochondrial succinate dehydrogenase is quantified using the MTT Assay. A colorimetric method was used to estimate this. Assuming that dead cells or their remains do not aid in the reduction of tetrazolium, this assay depends on the metabolic activity of living cells. MTT is converted into a dark purple formazan crystal inside the cell, mostly in the mitochondria. After Dimethyl Sulfoxide (DMSO)-assisted cell lysis, the solubilized formazan is measured spectrophotometrically at 570 nm to determine cell viability. Hela cells should be seeded in 96-well plates with 5000–10,000 cells per well and 100 μ L of complete growth medium. Incubate the cells for 24 h at 37°C in a humidified environment with 5% carbon dioxide (CO_2) to help them adhere to one another and grow. Make a stock solution of the test chemicals in DMSO or the suggested solvent at the proper concentrations. To reach the required final concentrations, dilute the stock solutions in full growth medium. Fill the corresponding cell-containing wells with the test chemical solutions. For comparison, include control wells with untreated and vehicle solvent-treated cells. Considering the experimental design and the compound's expected cytotoxicity profile, incubate the test compounds on the cells for a set period of time (often 24–72 h). After the incubation period, create an MTT solution by dissolving MTT in phosphate-buffered saline until the final concentration reaches 0.5 mg/ μ L. Fill each well-containing chemicals and cells with 10 μ L of MTT solution. To allow living

cells to convert the MTT into formazan crystals, incubate the plates at 37°C for 2–4 h. Pour 100 μ L of DMSO into each well to dissolve the formazan crystals produced by living cells. Give the plates a gentle shake for 10–15 min to ensure complete solubilization. Determine the absorbance of the formazan solution at 570 nm using a microplate reader (with a reference wavelength at 630 nm). Use the following formula to determine the percentage of cell viability in comparison to control wells:

$$\% \text{Inhibition} = \frac{100 (\text{Control} - \text{Treatment})}{\text{Control}}$$

The IC₅₀ value was determined by applying the linear regression equation, $y = mx + c$. The viability graph yielded the values of m, c, and $y = 50$.

3. RESULTS AND DISCUSSIONS

3.1. XRD Studies of Cd Substituted Al Nanoparticles (NPs)

XRD is essential for studying crystalline materials like chromites due to its ability to identify phases, determine crystallinity, and provide structural insights. Chromites, which often exhibit spinel structures, have distinct diffraction patterns that help confirm phase purity. Figure 2 indicates the XRD pattern of Cd doped Al nano chromites synthesized by citrate gel auto combustion method. The XRD patterns show distinct peaks corresponding to crystalline phases, providing insights into the structural and compositional nature of these materials. The consistent peak positions among all samples suggest that the primary structure is shared, while variations in peak intensity and sharpness indicate differences in crystallinity, phase purity, or microstructural properties. The observed peaks are characteristic of a spinel structure, which is typical for chromite-based materials. The spinel phase crystallizes in the cubic system with the space group Fd3m, where metal ions occupy tetrahedral and octahedral positions in the oxygen framework [15,16]. Peaks at low 2 θ angles, such as ~19°, ~30°, and ~36°, correspond to the (111), (220), and (311) planes, respectively [17]. Slight shifts in peak positions among the patterns can be attributed to variations in the Cd and Al composition, as the substitution of larger Cd ions affects the lattice parameters. While the spinel phase dominates, some patterns exhibit additional peaks or changes in peak shapes, indicating the possible presence of secondary phases. These could include FCC-type structures, such as Cd-O, which might form due to the segregation of

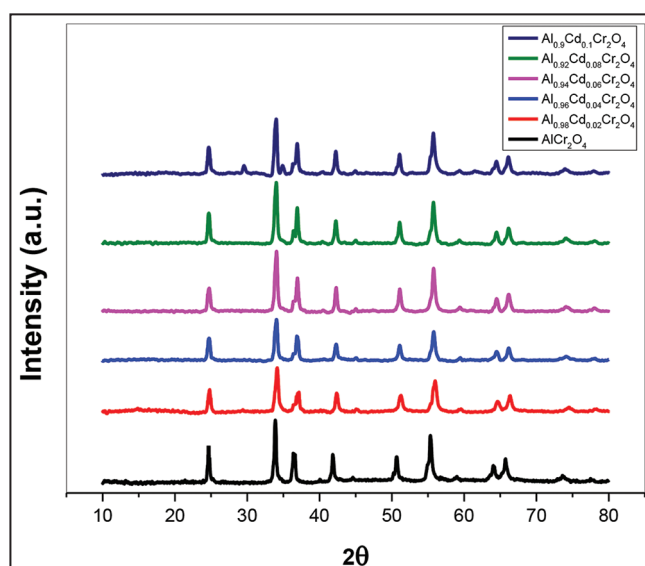


Figure 2: X-ray diffraction pattern of $Al_{1-x}Cd_xCr_2O_4$ where $x = 0.00, 0.02, 0.04, 0.06, 0.08$, and 0.10 .



Cd under specific synthesis conditions [18].

The average crystalline size(D) of the prepared Cd doped Al chromites were determined by using the Debye-Scherrer equation.

$$\text{Average crystalline size}(d) = \frac{0.94\lambda}{\beta \cos\theta}, \text{ Where } \lambda \text{ is wavelength, } \beta \text{ is the full-width half maxima, and } \theta \text{ is Brags angle.}$$

Figure 3 illustrates the average crystalline size versus lattice parameter of Al-Cd nano chromites prepared by citrate gel auto combustion method. The crystalline size of Cd-doped Al nano chromites demonstrates a distinct trend as the Cd composition increases. Initially, the crystalline size increases, peaking at a composition of around 0.04. This increase can be attributed to the effective grain growth facilitated by the substitution of Cd ions into the Al_2O_3 matrix. During this phase, the doping of Cd reduces lattice strain, allowing for more ordered and larger crystal formation. However, beyond the peak, the crystalline size starts to decrease slightly and stabilizes at higher Cd compositions. This reduction may result from the introduction of lattice defects, such as vacancies and dislocations, caused by the excessive doping of Cd ions, which disrupts the crystalline order and limits further growth. Lattice parameter of the samples was calculated by the following equation. $\text{Lattice parameter } (a) = d\sqrt{h^2 + k^2 + l^2}$ Whereas d refers interplanar distance and hkl indicates the Miller indices. The lattice parameter of Cd-doped Al decreases consistently with increasing Cd composition. This trend is primarily due to the ionic radius difference between Al^{3+} (0.53 Å) and Cd^{2+} (0.95 Å). When larger Cd^{2+} ions replace smaller Al^{3+} ions in the lattice, the overall structure experiences a contraction as it adjusts to accommodate the substitution. This decrease in lattice parameter suggests a systematic and homogeneous incorporation of Cd ions into the AlCr_2O_4 matrix. The observed behavior aligns with Vegard's law, where lattice parameters change linearly with the composition of a dopant, reflecting a well-integrated solid solution. The structural changes in both crystalline size and lattice parameter confirm the successful doping of Cd into the AlCr_2O_4 lattice [19].

Figure 4 shows unit cell volume and X-ray density variation of $\text{Al}_{1-x}\text{Cd}_x\text{Cr}_2\text{O}_4$ nanocrystals. Where x = 0.00, 0.02, 0.04, 0.06, 0.08, and 0.10 of Al-Cd nano chromites prepared by citrate gel auto combustion method. The volume of the unit cell for Cd-doped AlCr_2O_4 initially increases with increasing Cd composition, reaching a peak around a composition of 0.04. Beyond this point, the volume remains relatively stable. The initial increase can be attributed to the replacement of smaller Al^{3+} ions (ionic radius 0.53 Å) with larger Cd^{2+} ions (ionic radius 0.95 Å) in the AlCr_2O_4 lattice. The larger ionic size of Cd^{2+} leads to lattice expansion, increasing the unit cell volume. The X-ray density decreases steadily as the Cd composition increases. This behavior is due to the substitution of Al^{3+} ions with Cd^{2+} ions, which have a higher atomic weight but a larger ionic radius. The increase in unit cell volume due to lattice expansion outweighs the increase in mass caused by the addition of heavier Cd ions, leading to an overall decrease in X-ray density. The lattice expansion and reduced density can significantly affect the material's properties, the XRD parameter shown in Table 1.

3.2. SEM and Energy Dispersive Spectroscopy (EDS) Studies

Field Emission Scanning Electron Microscopy (FESEM) is a critical tool for analyzing the morphology and surface features of nanomaterials, including nano chromites. FESEM provides nanometer-scale resolution, essential for observing the fine morphological details of nanomaterials. It reveals the shape, size, and distribution of nanostructures, such as particles, and rods, crucial for understanding synthesis outcomes and their correlation with properties. FESEM visualizes surface textures, porosity, and agglomeration, which directly impact the material's performance in applications such as photocatalysis or sensors. It provides an accurate measure of particle size and uniformity, which is vital for determining the material's nanoscale behavior. Figure 5a-f indicates the FESEM images of synthesized Cd-doped Al nano chromites. The particles appear as aggregated, rod-like structures with rough surfaces. The rods seem to vary in size, with lengths approximately 100–200 nm, confirming their nanoscale dimensions. The particles show some degree of agglomeration, which is common in nanomaterials due to high surface energy. This could influence properties like surface area and catalytic performance. The roughness observed on the particle surfaces suggests a high degree of

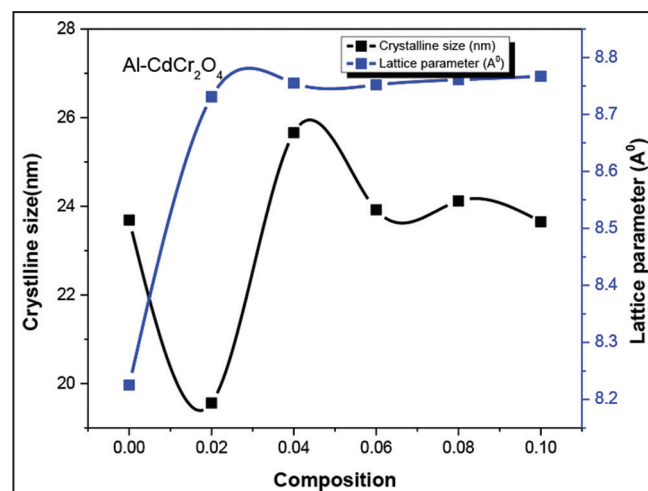


Figure 3: The variation of crystalline size and lattice parameter of $\text{Al}_{1-x}\text{Cd}_x\text{Cr}_2\text{O}_4$, with x values of 0.00, 0.02, 0.04, 0.06, 0.08, and 0.10 nano chromites.

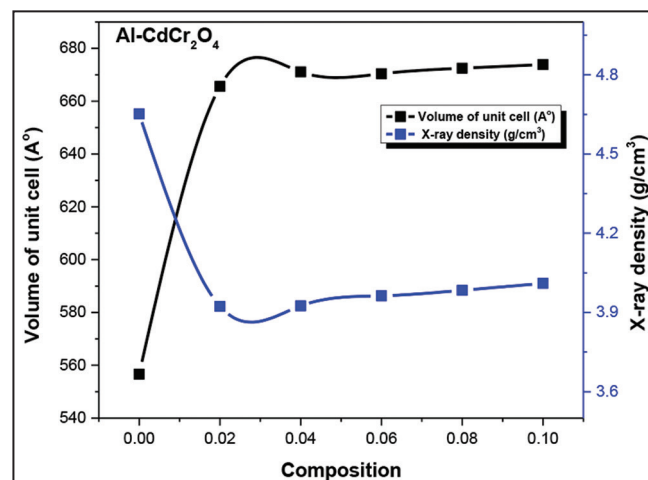
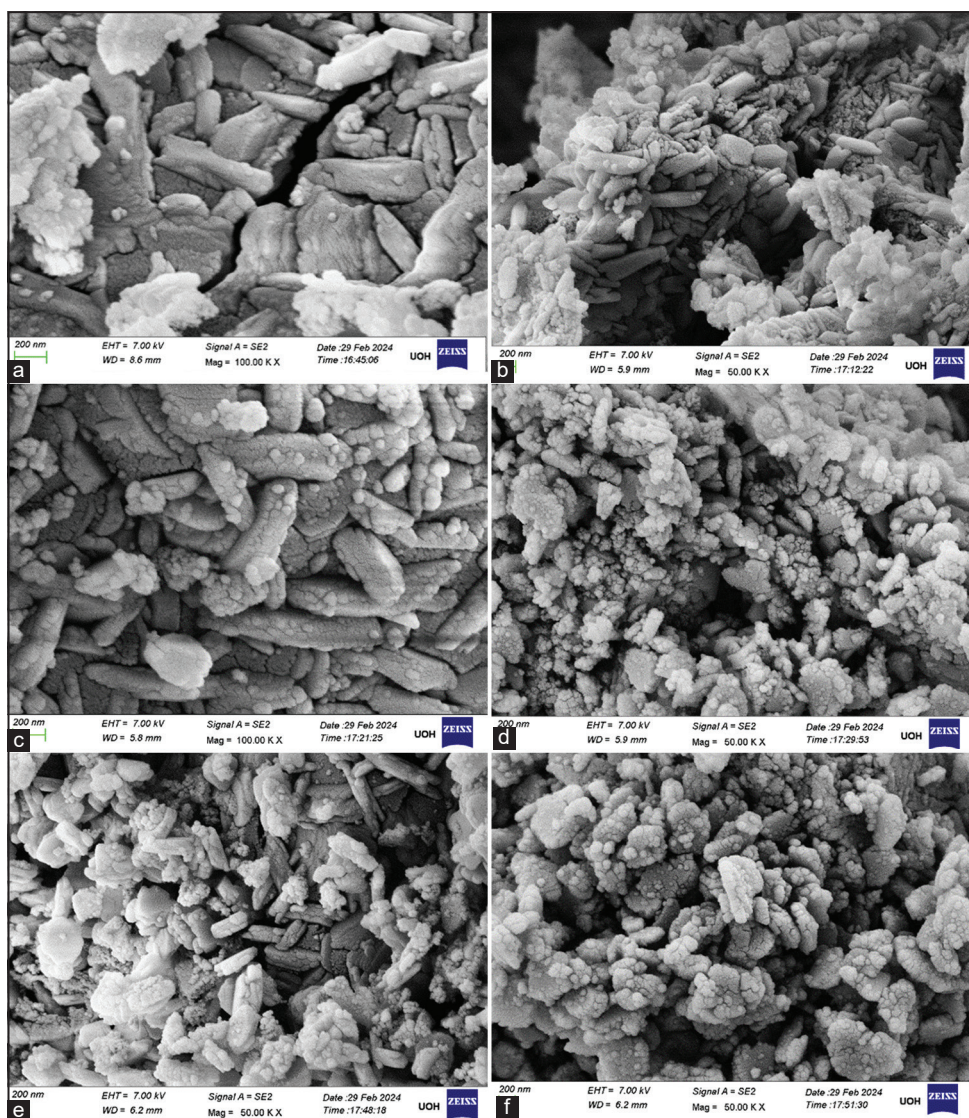


Figure 4: Unit cell volume and X-ray density variation of $\text{Al}_{1-x}\text{Cd}_x\text{Cr}_2\text{O}_4$ nanocrystals. Where x = 0.00, 0.02, 0.04, 0.06, 0.08, and 0.10.

Table 1: Crystalline size, lattice parameter, volume of unit cell, and x-ray density $\text{Al}_{1-x}\text{Cd}_x\text{Cr}_2\text{O}_4$ where $x=0.00, 0.02, 0.04, 0.06, 0.08$, and 0.10 nano chromites

Composition	Crystalline size (nm)	Lattice parameter (Å)	Volume of unit cell (Å)	X-ray density (g/cm³)	Cutoff wavelength (nm)	Band gap energy (eV)
AlCr_2O_4	23.69	8.225	556.607	4.652	440	2.21
$\text{Al}_{0.98}\text{Cd}_{0.02}\text{Cr}_2\text{O}_4$	19.56	8.731	665.581	3.923	437	2.83
$\text{Al}_{0.96}\text{Cd}_{0.04}\text{Cr}_2\text{O}_4$	25.66	8.755	671.082	3.925	424	2.90
$\text{Al}_{0.94}\text{Cd}_{0.06}\text{Cr}_2\text{O}_4$	23.92	8.752	670.391	3.963	418	2.96
$\text{Al}_{0.92}\text{Cd}_{0.08}\text{Cr}_2\text{O}_4$	24.12	8.761	672.466	3.984	423	2.93
$\text{Al}_{0.9}\text{Cd}_{0.1}\text{Cr}_2\text{O}_4$	23.65	8.767	673.855	4.010	440	2.81

**Figure 5:** (a-f) Scanning electron microscopy images of $\text{Al}_{1-x}\text{Cd}_x\text{Cr}_2\text{O}_4$ nanocrystals. Where $x = 0.00, 0.02, 0.04, 0.06, 0.08$, and 0.10 .

crystallinity or possible porosity, which may enhance applications such as photocatalysis by increasing active surface area [20]. The image indicates successful synthesis of rod-like nanostructures.

EDS is a powerful analytical technique that provides elemental composition analysis for materials, including nanomaterials. EDS identifies and quantifies the elements present in a nanomaterial. This is critical for confirming the intended composition of synthesized

materials, such as metal oxides or doped nanostructures. EDS helps detect unintended impurities or residual elements from synthesis processes, ensuring the purity of the nanomaterial. EDS verifies the stoichiometric ratio of elements, ensuring proper formation. EDS is fast, non-destructive, and compatible with most nanomaterials, making it a versatile tool for routine characterization. Figure 6a-l represents the energy dispersive spectrum of Cd doped Al nano chromites prepared by citrate gel auto combustion method. The

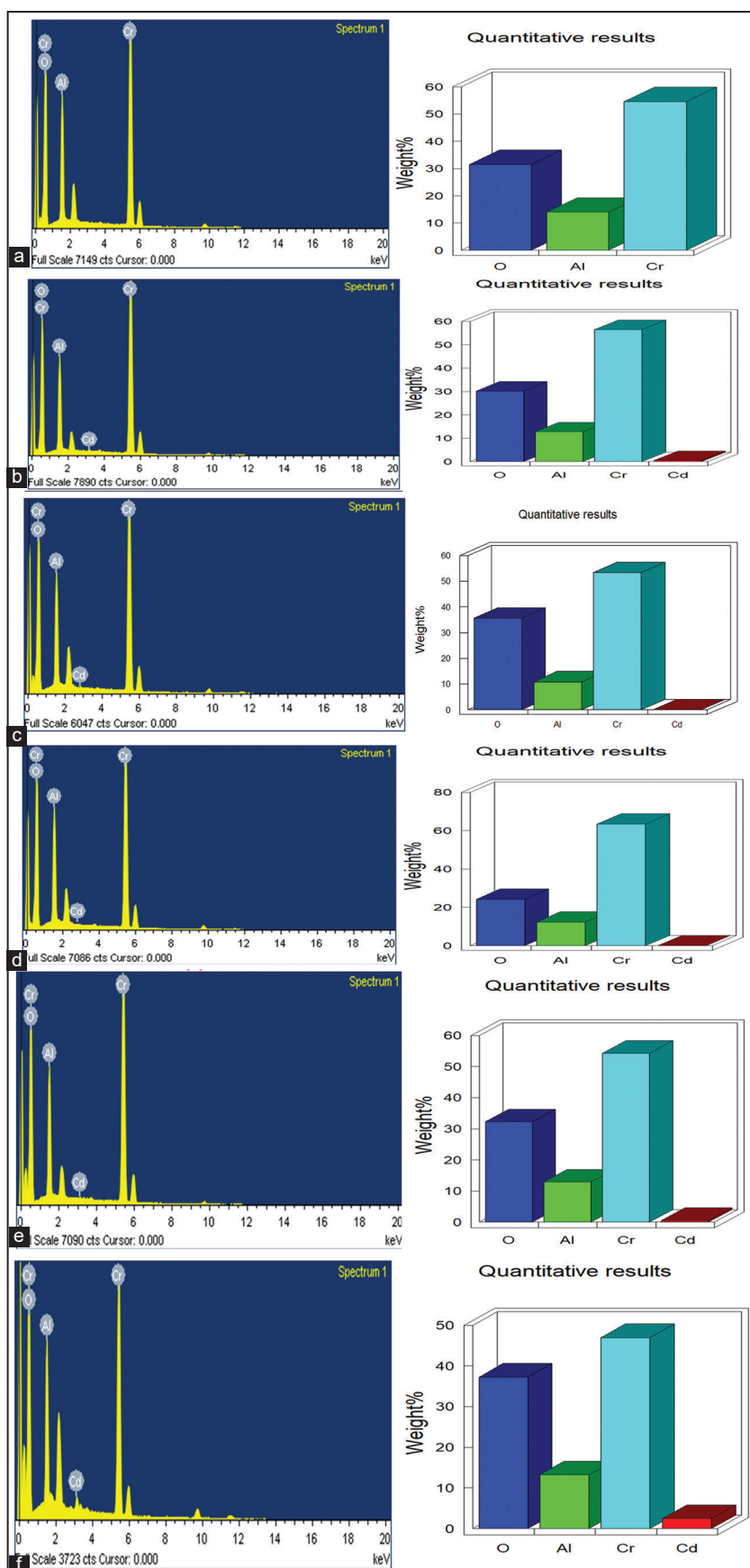


Figure 6: (a-f) EDS graphs of $\text{Al}_{1-x}\text{Cd}_x\text{Cr}_2\text{O}_4$ nanocrystals. Where $x = 0.00, 0.02, 0.04, 0.06, 0.08$, and 0.10 .

resultant EDS spectrum contains Cd, Al, Cr, and O elemental composition of a sample. The spectrum confirms the presence of chromium oxide with possible contributions from Al and Cd. This information is critical for confirming synthesis outcomes and assessing material composition.

3.3. FTIR Spectroscopy

FTIR spectroscopy is a vital tool in nanomaterials research as it provides detailed insights into their chemical composition, functional groups, and molecular interactions. It is essential for confirming the presence of specific functional groups, such as metal-oxygen (M–O) bonds in metal oxides, and identifying surface modifications or residual impurities from synthesis processes. FTIR also aids in studying the interactions between nanomaterials and other substances, such as in nanocomposites, and helps monitor changes in functional groups during thermal or chemical treatments. Figure 7a-f indicates the FTIR spectrum of $\text{Al}_{1-x}\text{Cd}_x\text{Cr}_2\text{O}_4$ nanocrystals. Where $x = 0.00, 0.02, 0.04, 0.06, 0.08$, and 0.10 . The bands in the 400 cm^{-1} and 600 cm^{-1} wavenumber domain in the FTIR spectra of chromites (such as spinel oxides) correspond to the characteristic vibrations of cations in octahedral and tetrahedral sites of the spinel lattice. The 600 cm^{-1} band corresponds to the stretching vibration of metal-oxygen bonds in the tetrahedral sites ($\text{A}^{2+}\text{-O}$). These bonds are shorter and stronger due to the smaller coordination number (4) in the tetrahedral geometry, leading to higher vibrational frequencies. The

400 cm^{-1} band is associated with the stretching vibration of metal-oxygen bonds in the octahedral sites ($\text{B}^{3+}\text{-O}$) [21]. These bonds are longer and weaker compared to tetrahedral sites due to the higher coordination number (6), resulting in lower vibrational frequencies. The distinct positions of these bands help confirm the spinel structure of chromites.

3.4. Optical Studies of Cd Substitutes Al NPs

UV-visible spectroscopy is a vital technique for studying the optical properties of materials, offering insights into their light absorption behavior and electronic structure. The absorbance spectrum reveals the material's ability to absorb specific wavelengths, which is directly related to electronic transitions, such as the movement of electrons from the valence band to the conduction band. Figure 8 shows the UV-Vis spectrum of prepared $\text{Al}_{1-x}\text{Cd}_x\text{Cr}_2\text{O}_4$ where $x=0.00$ to 0.1 with 0.02 variation synthesized by citrate gel auto combustion method recorded from 200 nm to 700 nm wavelength range [22]. Absorbance of the material decreases as increasing the concentration of cadmium, the optical band gap energy was determined by using Tauc plots [23]. Changes in the absorption spectra, such as peak shifts or variations in intensity, indicate modifications in the material's structure, composition, or electronic properties. These studies are particularly significant for applications in photocatalysis, and photovoltaics devices, where the tailored optical properties enhance light-harvesting efficiency and performance.

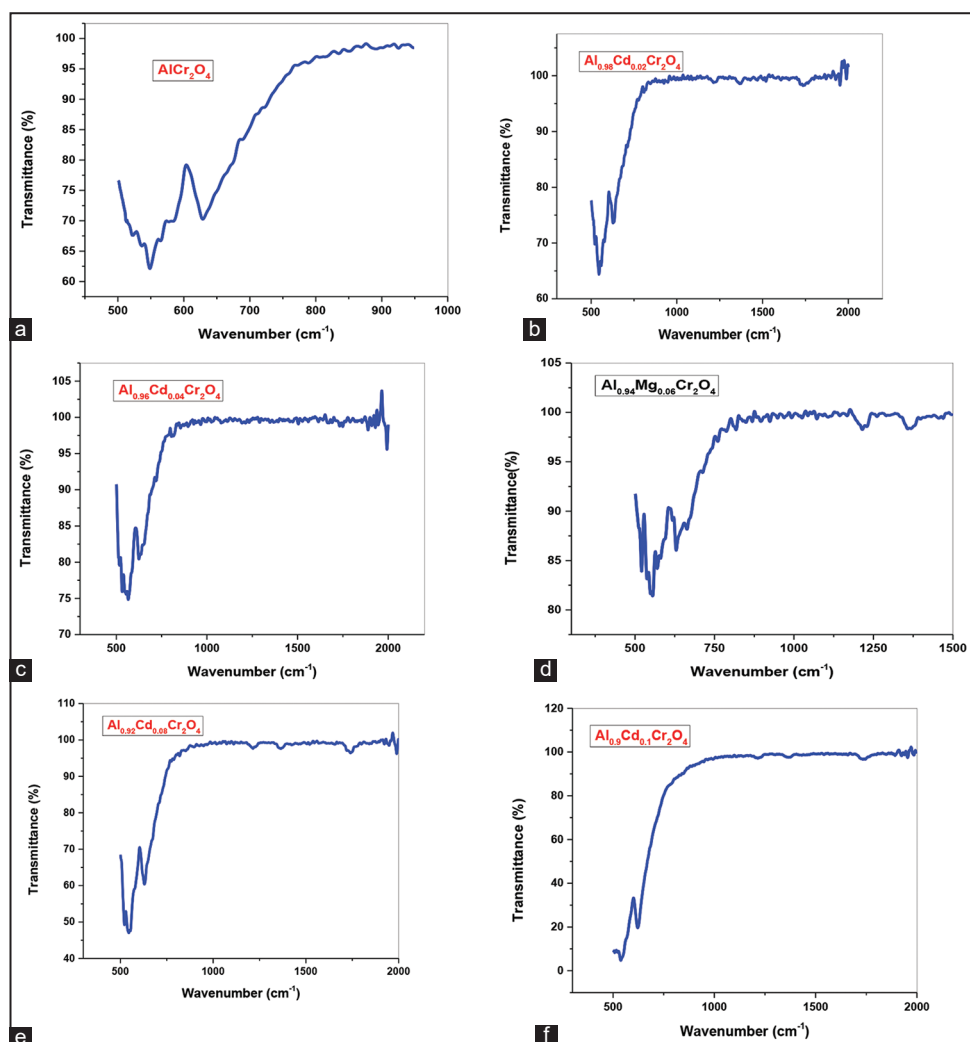


Figure 7: (a-f) Fourier-transform infrared spectrum of $\text{Al}_{1-x}\text{Cd}_x\text{Cr}_2\text{O}_4$ nanocrystals. Where $x = 0.00, 0.02, 0.04, 0.06, 0.08$, and 0.10 .

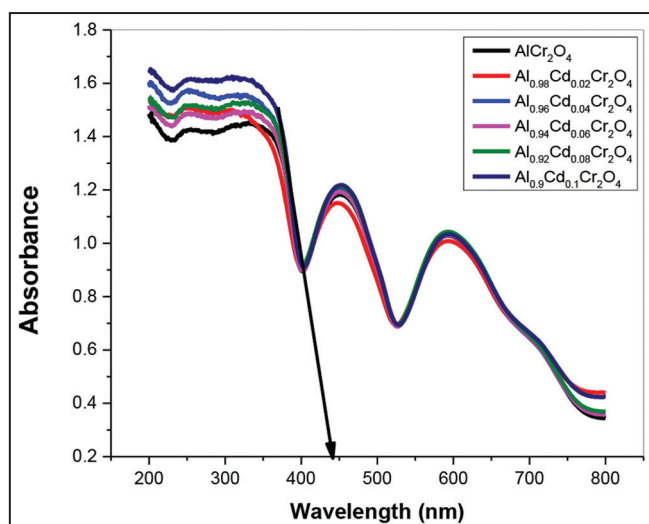


Figure 8: Ultraviolet-visible spectrum of $\text{Al}_{1-x}\text{Cd}_x\text{Cr}_2\text{O}_4$ nanocrystals. Where $x = 0.00, 0.02, 0.04, 0.06, 0.08$, and 0.10 .

The Tauc plots in Figure 9a-f illustrate the variation in optical band gap energy (E_g) for AlCr_2O_4 and its Cd-doped derivatives. The undoped AlCr_2O_4 exhibits a band gap of 2.21 eV, indicating its suitability for visible light absorption. With Cd doping, the band gap values vary systematically, reaching a maximum of 2.96 eV for Sample $\text{Al}0.94\text{Cd}0.06\text{Cr}_2\text{O}_4$ and a minimum of 2.33 eV for Sample $\text{Al}0.94\text{Cd}0.06\text{Cr}_2\text{O}_4$ [24]. This variation highlights the influence of Cd incorporation on the material's electronic structure, suggesting the potential tunability of optical properties. The trend indicates that moderate Cd doping increases the band gap, likely due to reduced defect density or structural modifications, while excessive doping reduces it, possibly due to lattice distortion or defect formation [25,26]. Such tunability makes these materials promising for optoelectronic applications.

3.5. PL Spectrum of Cd Substituted

PL spectroscopy is essential for studying the optical properties and electronic behavior of Cd-doped Al nano chromites. It provides insights into the material's electronic structure, including defect states, which are critical for applications such as photocatalysis and optoelectronics.

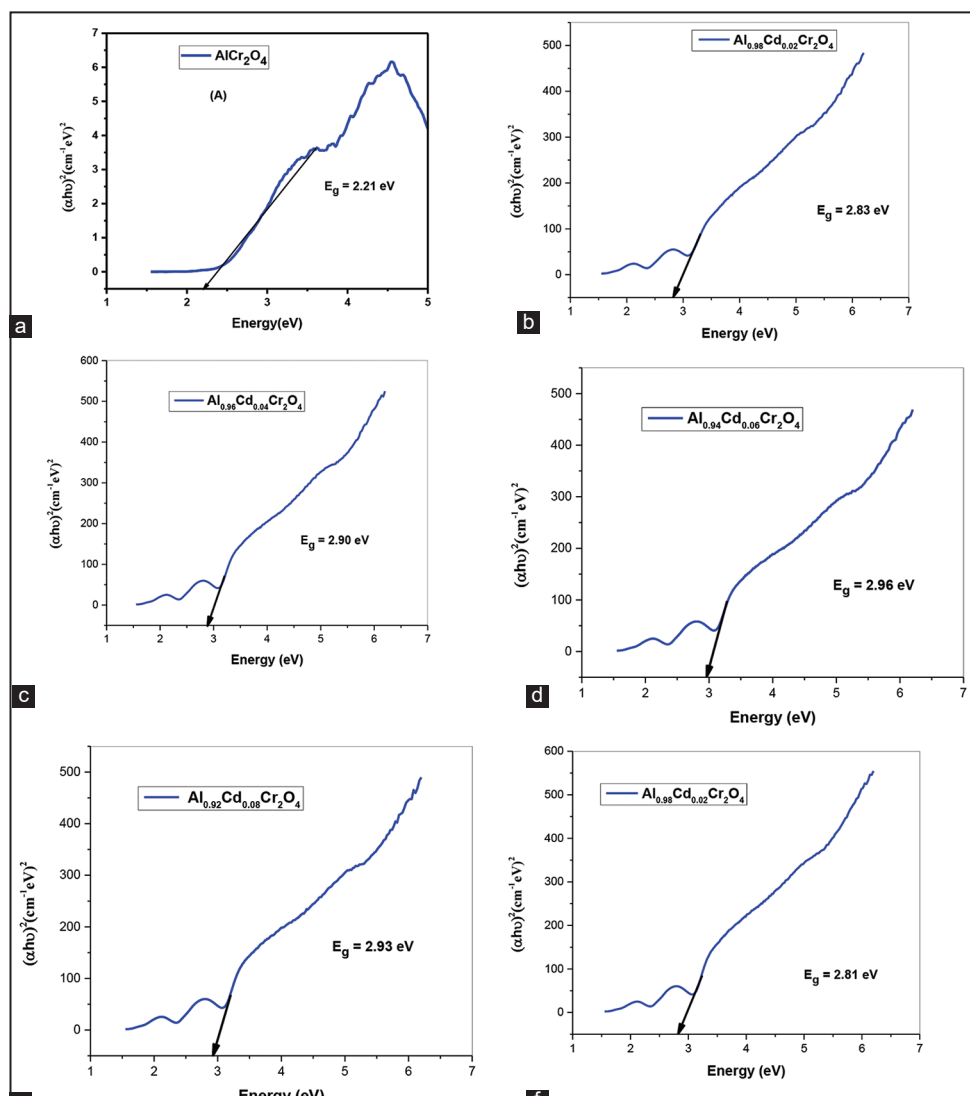


Figure 9: (a-f) Tauc's plots of $\text{Al}_{1-x}\text{Cd}_x\text{Cr}_2\text{O}_4$ nanocrystals. Where $x = 0.00, 0.02, 0.04, 0.06, 0.08$, and 0.10 .

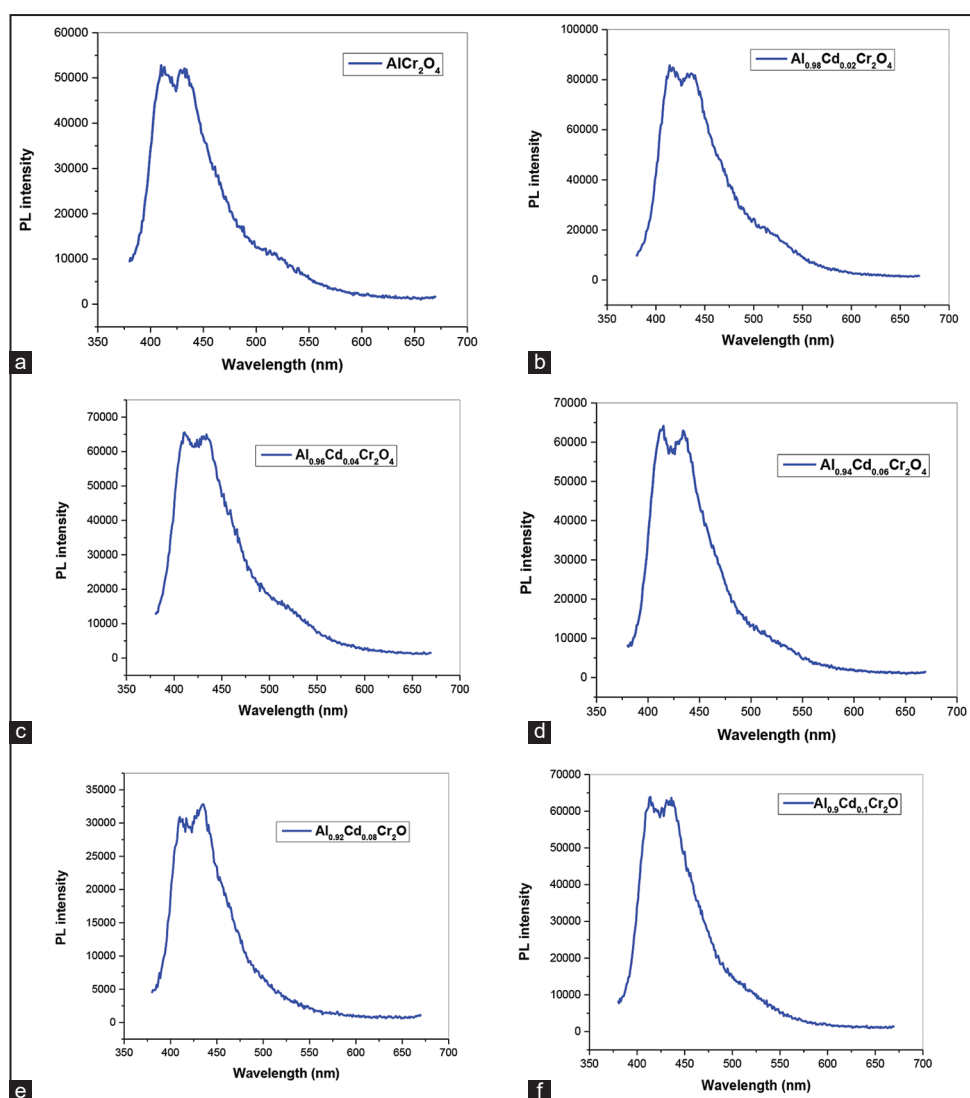


Figure 10: (a-f) Photoluminescence spectrum of $\text{Al}_{1-x}\text{Cd}_x\text{Cr}_2\text{O}_4$ nanocrystals. Where $x = 0.00, 0.02, 0.04, 0.06, 0.08$, and 0.10 .

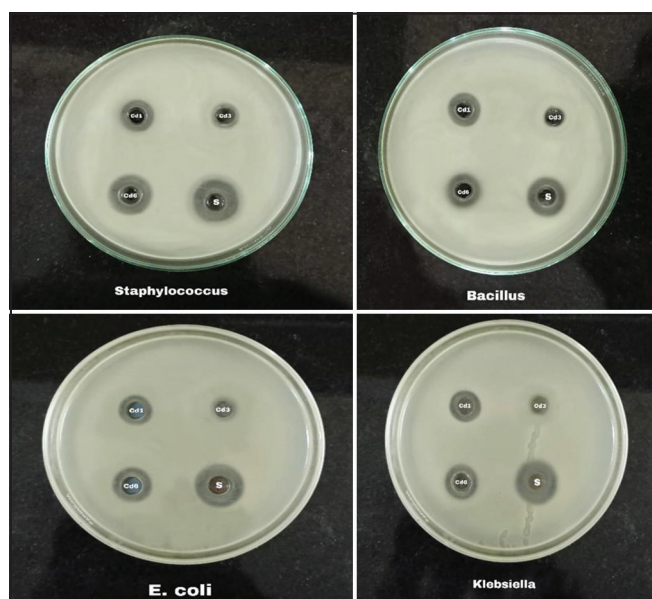


Figure 11: Antibacterial activity of $\text{Al}_{1-x}\text{Cd}_x\text{Cr}_2\text{O}_4$ where $x = 0.00, 0.04$, and 0.10 nano chromites against *Staphylococcus* and *Bacillus*.

The technique helps assess the impact of Cd and Al on charge carrier dynamics by analyzing recombination rates of photogenerated electrons and holes, with weaker PL intensity indicating enhanced charge separation and better photocatalytic efficiency [27,28].

The spectrum Figure 10a-f shows a broad PL emission in the range of approximately 400–470 nm, peaking near 450 nm. This suggests a strong emission in the blue region of the visible spectrum. With an excitation wavelength of 350 nm (UV region), the emission indicates radiative recombination of photoexcited charge carriers. The peak around 450 nm corresponds to electronic transitions, likely involving energy states influenced by the Al and Cd dopants. The broadness of the peak indicates the presence of defect states in the material. These may include oxygen vacancies, Cr^{3+} energy levels, or dopant-induced trap states, which act as intermediate energy levels between the conduction and valence bands [29]. The high PL intensity indicates significant radiative recombination of electrons and holes. While this is favorable for luminescent applications, it may suggest limited charge separation, which could impact photocatalytic efficiency.

3.6. Antibacterial Activity of Al-Cd Nano Chromites

Antibacterial activity is of critical importance in various fields, including medicine, agriculture, and environmental science, as it directly addresses

the challenge of bacterial infections and contamination. Antibacterial activity of the synthesized Cd-Al nano chromites tested against four bacterial agents two Gram-positive (*Bacillus* and *Staphylococcus*) and two Gram-negative (*Klebsiella* and *E. coli*) bacterial agents [30]. Figure 11 shows the zone of inhibition images of Cd-substituted Al nano chromites against bacterial agents. The images represent an agar diffusion test performed to evaluate the antimicrobial activity of different samples against the bacterial strain *Bacillus*, *Staphylococcus*, *Klebsiella*, and *E. coli*. Clear zones of inhibition are observed around the disks, indicating the extent to which each sample inhibits bacterial growth. The sizes of these zones vary, suggesting differences in the antimicrobial efficacy of the respective samples. This comparative test provides insights into the potential of the samples as antimicrobial agents, with larger zones of inhibition reflecting higher activity [31]. Table 2 shows the zone of inhibition values of the antimicrobial activity of Cd-doped Al nano chromates against Gram-positive (*Staphylococcus* and *Bacillus*) and Gram-negative (*E. coli* and *Klebsiella*) bacterial pathogens. The zone of inhibition, measured in millimeters, indicates the effectiveness of each sample in inhibiting bacterial growth. Among the tested samples, AlCr_2O_4 and $\text{Al}_{0.9}\text{Cd}_{0.1}\text{Cr}_2\text{O}_4$ show activity.

Table 3 shows the MIC values analysis of the antibacterial efficacy of Cd-doped Al nano chromites, synthesized through the citrate gel auto-combustion method, against four bacterial strains: *Staphylococcus*, *Bacillus*, *E. coli*, and *Klebsiella*. Two types of nanoparticles, Cd-1 and Cd-6, were tested at varying concentrations (25 μL , 50 μL , 75 μL , and 100 μL), and their effects were measured in terms of the inhibition zone diameter (in mm) and the minimum inhibitory concentration (MIC). Figure 12 indicates the minimum inhibition concentration (MIC) of $\text{Al}_{1-x}\text{Cd}_x\text{Cr}_2\text{O}_4$ where $x = 0.00, 0.04$, and 0.10 nano chromites against *Staphylococcus*, *Bacillus*, *E. coli*, and *Klebsiella*. Cd-1 exhibited

antibacterial activity across all tested organisms, with an MIC of 75 μL for *Staphylococcus*, *Bacillus*, and *E. coli*, and a slightly higher MIC of 100 μL for *Klebsiella*. Similarly, Cd-6 showed effective activity against *Staphylococcus* (MIC = 50 μL), *Bacillus* (MIC = 75 μL), and *Klebsiella* (MIC = 100 μL), but it showed no activity against *E. coli*. These results suggest that both Cd-1 and Cd-6 nanoparticles are effective antibacterial agents, with varying potency depending on the bacterial strain and the nanoparticle type.

3.7. Antifungal Activity of Al-Cd NPs

Figure 13 illustrates zone of inhibition of antifungal activity of Cd-Al nano chromates against two fungal strains: *Aspergillus* and *Candida*. In the Aspergillus plate, clear inhibition zones are observed around the Cd-1 indicating their antifungal activity, though the size of the zones suggests variation in efficacy among the nanoparticles. Similarly, the *Candida* plate shows inhibition zones around Cd-1 and Cd-6, confirming their effectiveness against this strain as well. Table 4 presents the antifungal activity of Cd-doped Al nano chromates against *Candida* and *Aspergillus*, measured as zones of inhibition in millimeters. Among the tested samples, Cd-1 exhibited a 10 mm inhibition zone against *Candida* but showed no activity against *Aspergillus*. Cd-3 demonstrated no antifungal activity against either fungal strain. Cd-6 was effective against both pathogens, with a 10 mm inhibition zone for *Candida* and *Aspergillus* [32].

Table 5 shows the MIC values derived from the analysis of antifungal activity of cadmium substituted Al nano chromites. For Cd-1 nanoparticles, the MIC against *Candida* was recorded at 50 μL , showing an inhibition zone of 8 mm at both 50 μL and 75 μL concentrations and 10 mm at 100 μL . *Aspergillus*, however, exhibited no observable

Table 2: Zone of inhibition values of Cd doped Al nano chromates nano against Gram-positive and Gram-negative bacterial pathogens

S. No.	Sample Name	Gram-positive bacterial pathogens		Gram-negative bacterial pathogens	
		Zone of inhibition (mm)		Zone of inhibition (mm)	
		<i>Staphylococcus</i>	<i>Bacillus</i>	<i>Escherichia coli</i>	<i>Klebsiella</i>
1.	Cd-1 (AlCr_2O_4)	08 mm	08 mm	08 mm	08 mm
2.	Cd-3	-	-	-	-
3.	Cd-6 ($\text{Al}_{0.9}\text{Cd}_{0.1}\text{Cr}_2\text{O}_4$)	08 mm	07 mm	08 mm	08 mm
4.	Standard	14 mm	10 mm	12 mm	12 mm

Cd: Cadmium, Al: Aluminum

Table 3: MIC analysis of antibacterial activity (*Staphylococcus*, *Bacillus*, *E. coli*, and *Klebsiella*) against of Cd doped Al nano chromates nano chromates by citrate gel auto combustion method

S. No.	Name of organism	Name of the nanoparticles	Concentration of samples				MIC of sample (μL)
			25 μL	50 μL	75 μL	100 μL	
1.	<i>Staphylococcus</i>		-	-	08 mm	10 mm	75 μL
2.	<i>Bacillus</i>		-	-	08 mm	10 mm	75 μL
3.	<i>E. coli</i>	Cd-1			08 mm	10 mm	75 μL
4.	<i>Klebsiella</i>	(AlCr_2O_4)				10 mm	100 μL
5.	<i>Staphylococcus</i>			08 mm	10 mm	12 mm	50 μL
6.	<i>Bacillus</i>				08 mm	08 mm	75 μL
7.	<i>E. coli</i>	Cd-6	-	-	-	-	-
8.	<i>Klebsiella</i>	($\text{Al}_{0.9}\text{Cd}_{0.1}\text{Cr}_2\text{O}_4$)				10 mm	100 μL

E. coli: *Escherichia coli*, Cd: Cadmium, Al: Aluminum

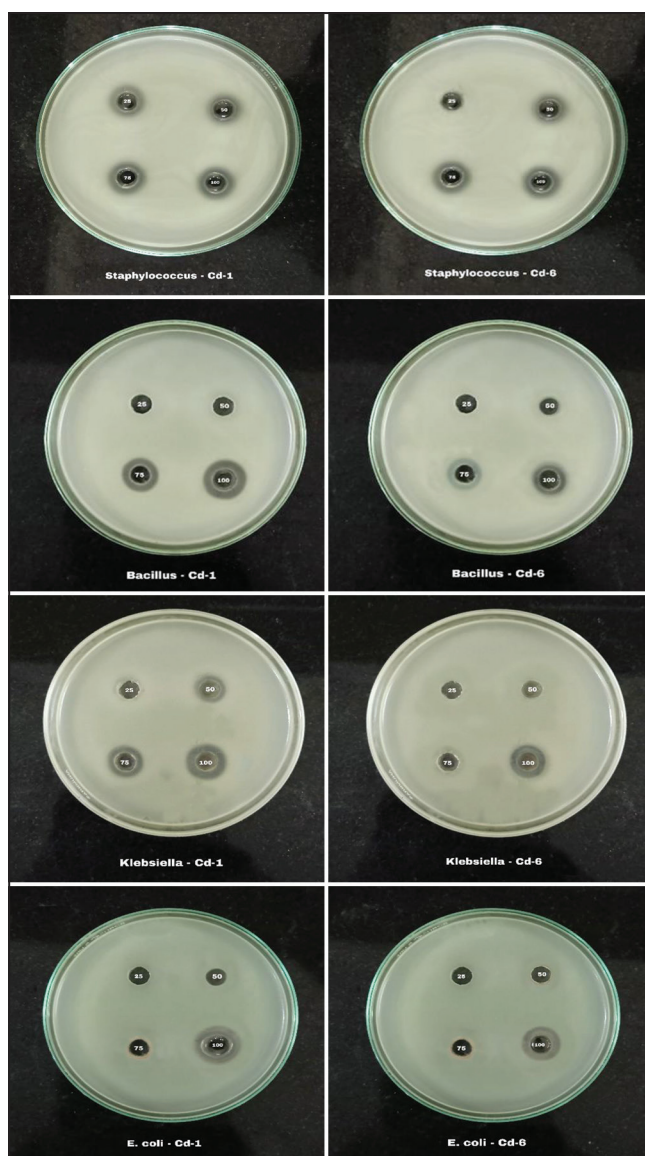


Figure 12: Minimum inhibition concentration (MIC) of $\text{Al}_{1-x}\text{Cd}_x\text{Cr}_2\text{O}_4$ where $x = 0.00, 0.04$, and 0.10 nano chromites against *staphylococcus*, *Bacillus*, *Escherichia coli*, and *Klebsiella*.

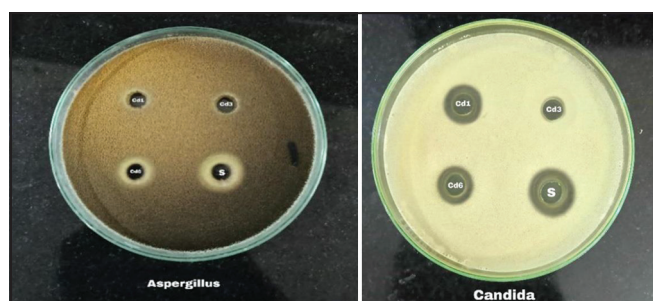


Figure 13: Anti-fungal activity (*Aspergillus* and *Candida*) of $\text{Al}_{1-x}\text{Cd}_x\text{Cr}_2\text{O}_4$ where $x = 0.00, 0.04$, and 0.10 nano chromites.

inhibitory activity against Cd-1. For Cd-6 nanoparticles, *Aspergillus* demonstrated an MIC of $100 \mu\text{L}$, producing a 10 mm inhibition zone at that concentration. Figure 14 illustrates the minimum inhibition concentration (MIC) of $\text{Al}_{1-x}\text{Cd}_x\text{Cr}_2\text{O}_4$ where $x = 0.00, 0.04$, and 0.10 nano chromites against *Aspergillus* and *Candida*. In contrast, *Candida* showed antifungal activity with an MIC of $50 \mu\text{L}$, producing inhibition zones of 8 mm at both $50 \mu\text{L}$ and $75 \mu\text{L}$ and 12 mm at $100 \mu\text{L}$. These

Table 4: Zone of inhibition values of Cd^{2+} -doped Al nano chromates against *Candida* and *Aspergillus*

S. No.	Sample name	Fungal pathogens	
		Zone of inhibition (mm)	
		<i>Candida</i>	<i>Aspergillus</i>
1.	Cd-1	10 mm	-
2.	Cd-3	--	-
3.	Cd-6	10 mm	10 mm
4.	Standard	12 mm	10 mm

Cd: Cadmium, Al: Aluminum

results highlight the potential of Cd-doped Al nano chromates as antifungal agents, particularly against *Candida* with Cd-6 nanoparticles.

3.8. Anti-cancer Activity of Cd Doped Al Chromite Particles

Inorganic nanoparticles, especially nano chromites, have been researched for potential biomedical uses in recent years. HeLa

cells, a proven model for studying human cervical cancer, were used to analyze samples of Cd²⁺ doped Al nano chromites for their anticancer properties. HeLa cells are usually kept in a CO₂ incubator and are grown under carefully regulated laboratory settings, which include the provision of an ideal growth medium,

temperature, and humidity. When compared to untreated control cells, the evaluation of cell viability a critical component of the study is frequently expressed as either relative vitality or percentage viability [33]. Half-maximal inhibitory concentration (IC₅₀) values, which show the concentration at which a substance suppresses cell

Table 5: MIC analysis of antibacterial activity (*Staphylococcus*, *Bacillus*, *E. coli*, and *Klebsiella*) against of Cd doped Al nano chromates

S. No.	Name of organism	Name of the Nanoparticles	Concentration of samples				MIC of sample (μL)
			25 μL	50 μL	75 μL	100 μL	
1.	<i>Aspergillus</i>	Cd-1 (AlCr ₂ O ₄)	-	-	-	-	50 μL
2.	<i>Candida</i>		-	08 mm	08 mm	10 mm	--
1.	<i>Aspergillus</i>	Cd-6 (Al _{0.9} Cd _{0.1} Cr ₂ O ₄)			10 mm		100 μL
2.	<i>Candida</i>			08 mm	08 mm	12 mm	50 μL

Cd: Cadmium, Al: Aluminum

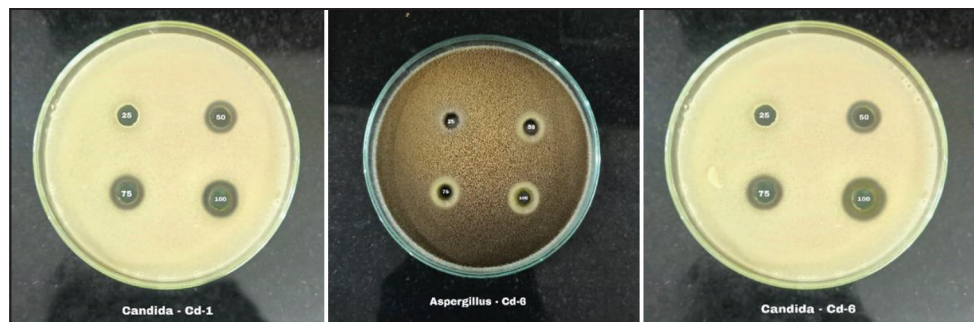


Figure 14: Minimum inhibition concentration (MIC) of Al_{1-x}Cd_xCr₂O₄ where x = 0.00, 0.04, and 0.10 nano chromites against *Aspergillus* and *Candida*.

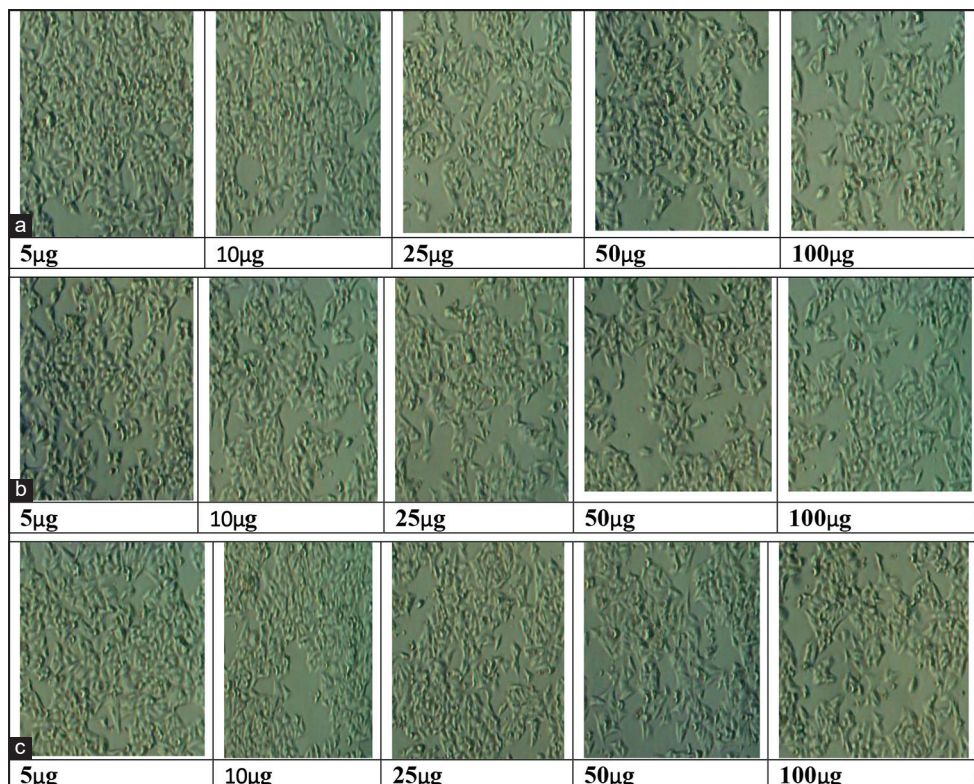
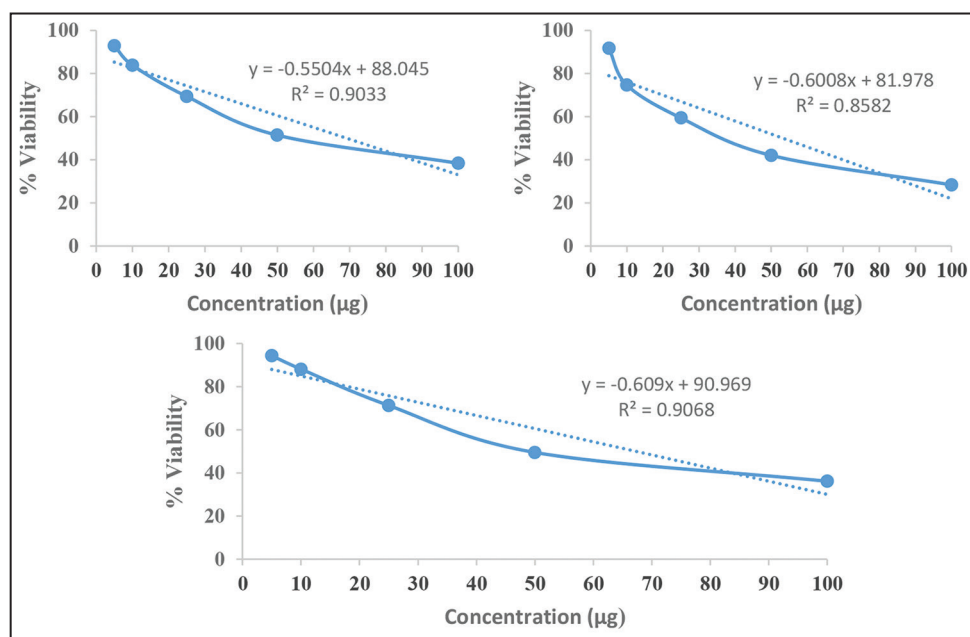


Figure 15: (a) Cell viability of AlCr₂O₄ nano chromites against Hela cell. (b) Cell viability of Al_{0.96}Cd_{0.04}Cr₂O₄ nano chromites against Hela cell. (c) Cell viability of Al_{0.9}Cd_{0.1}Cr₂O₄ nano chromites against Hela cell.

Table 6: Hela cells were treated with $\text{Al}_{1-x}\text{Cd}_x\text{Cr}_2\text{O}_4$ where $x=0.04$, and 0.10 nano chromites of Absorbance, % inhibition, viability, and IC_{50} values

S. No.	Name of the sample	Concentration (mg)	Absorbance at 570nm	Percentage (%) of inhibition	Percentage (%) of Viability	IC_{50} (mg)
1.	Cd-1	5	0.584	7.15	92.85	69.12
2.		10	0.527	16.21	83.79	
3.		25	0.436	30.68	69.32	
4.		50	0.323	48.64	51.36	
5.		100	0.241	61.68	38.32	
6.		Untreated	0.629	0	100	
7.		Blank	0	0	0	
1.	Cd-3	5	0.576	8.42	91.58	53.22
2.		10	0.469	25.43	74.57	
3.		25	0.373	40.69	59.31	
4.		50	0.264	58.02	41.98	
5.		100	0.178	71.70	28.3	
6.		Untreated	0.629	0	100	
7.		Blank	0	0	0	
1.	Cd-6	5	0.593	5.72	94.28	67.27
2.		10	0.554	11.92	88.08	
3.		25	0.448	28.77	71.23	
4.		50	0.311	50.55	49.45	
5.		100	0.227	63.91	36.09	
6.		Untreated	0.629	0	100	
7.		Blank	0	0	0	

IC_{50} : Half-maximal inhibitory concentration

**Figure 16:** % of Cell viability of the $\text{Al}_{1-x}\text{Cd}_x\text{Cr}_2\text{O}_4$ where $x = 0.00, 0.04$, and 0.10 nano chromites.

viability by 50%, are calculated and the significance of observed effects is evaluated statistically. The cell viability of $\text{Al}_{1-x}\text{Cd}_x\text{Cr}_2\text{O}_4$ with $x = 0.0, 0.04$, and 0.10 nano chromites against Hela cells is displayed in Figure 15a-c.

Table 6 shows the anticancer activity of $\text{Al}_{1-x}\text{Cd}_x\text{Cr}_2\text{O}_4$ with $x = 0.0, 0.04$, and 0.10 nano chromites against HeLa cells was evaluated through MTT assay, measuring absorbance, percentage inhibition, and cell viability. Among the tested samples $\text{Al}_{0.96}\text{Cd}_{0.04}\text{Cr}_2\text{O}_4$ exhibited the highest potency with an IC_{50} value of 53.22, indicating

stronger inhibition of HeLa cell growth. At the highest concentration (100 mg), Cd-3 achieved 71.70% inhibition with only 28.30% cell viability, showing dose-dependent cytotoxicity. In comparison, Cd-1 and Cd-6 displayed moderate activity with IC₅₀ values of 69.12 mg and 67.27 mg, respectively. These results suggest that Cd-3 holds the most promise as an effective candidate for anticancer studies. Cancer cells, particularly HeLa cells, can easily absorb these nanoparticles due to their small size and special surface properties. Cd-doped Al nanoparticles show promise as a novel method for increasing the effectiveness of radiation therapy in cervical cancer, such as HeLa cells, because they specifically target cancer cells, intensify the effects of radiation therapy, and may even cause apoptosis in cancer cells while minimizing damage to healthy tissues. The % of cell viability of Al_{1-x}Cd_xCr₂O₄ with x = 0.0, 0.04, and 0.10 nano chromites against Hela cells at varying concentrations is shown in Figure 16.

4. CONCLUSIONS

Using the citrate gel auto combustion method, Al_{1-x}Cd_xCr₂O₄ with x = 0.00, 0.02, 0.04, 0.06, 0.08, and 0.10 calcinated temperature at 500°C has been successfully synthesized. The samples' crystalline sizes range from 19 nm to 25 nm, whereas lattice parameter values observed 8.225–8.767 Å. The SEM images would show the distribution of these sizes, providing details regarding the homogeneity. The 550 cm⁻¹ and 625 cm⁻¹ portion of the FTIR spectrum correspond to the Cr-O or Al-O stretching vibrations of the tetrahedral sites and the Cd-O octahedral sites, respectively. The addition of Cd ions to the AlCr₂O₄ matrix causes a systematic change in the trend of band gap energy values. Potential tunability for particular optoelectronic applications is indicated by the band gap modulation. The peak at 450 nm in the PL spectrum suggests defect-driven emission in the blue region, indicating successful Cd-Al doping in chromites. It is possible to modify the material's optical characteristics for use in blue-emitting luminous devices. The antibacterial activity of Al Cd nano chromites has been investigated against both Gram-positive and Gram-negative bacteria, such as *Staphylococcus* and *Bacillus*, as well as *Klebsiella* and *E. coli*. The lowest MIC value against *Staphylococcus* was reported to be 50 µL for Al_{0.9}Cd_{0.1}Cr₂O₄. *Candida* exhibited the biggest zone of inhibition (12 mm) in the Al_{0.9}Cd_{0.1}Cr₂O₄ sample.

5. ACKNOWLEDGMENT

Authors are thankful to department of chemistry for provided necessary facilities to carry out the research work.

6. DECLARATION

The authors declare that they have no known competing financial interests or personal relationships that could have appeared to influence the work reported in this paper.

REFERENCES

- N. R. Mamidipalli, P. Tiyyagura, S. Punna Rao, S. B. Kothamasu, R. Pothu, R. Boddula, N. Al-Qahtani, (2024) Crystallite size effects on electrical properties of nickel chromite (NiCr₂O₄) spinel ceramics: A study of structural, magnetic, and dielectric transitions, *ChemEngineering*, **8**: 100.
- M. Priyanka, Y. S. Vidya, H. C. Manjunatha, G. S. Reddy, T. R. K. Reddy, R. Munirathnam, S. Manjunatha, M. Shivanna, S. Kumar, E. Krishnakanth, (2024) Comparison of blue luminescence and supercapacitance properties of zinc chromite nanoparticles synthesized via chemical and green mediated approach, *Materials Science and Engineering: B*, **301**: 117190.
- Z. Mousavi, M. Esmaeili-Zare, M. Salavati-Niasari, (2015) Magnetic and optical properties of zinc chromite nanostructures prepared by microwave method, *Transactions of Nonferrous Metals Society of China*, **25**: 3980-3986.
- A. Sen, P. Pramanik, (2002) Preparation of nano-sized calcium, magnesium, and zinc chromite powder through metalo-organic precursor solutions, *Journal of Materials Synthesis and Processing*, **10**: 107-111.
- A. A. H. El-Bassouny, H. K. Abdelsalam, (2020) Synthesis, characterization, magnetic and antimicrobial properties of silver chromite nanoparticles, *Journal of Materials Science: Materials in Electronics*, **31**: 3662-3673.
- Y. Kou, P. Luo, L. Xiao, Y. Xin, G. Zhang, Y. Hu, J. Yang, H. Gao, F. Zhao, W. Jiang, G. Hao, (2024) New insights in nano-copper chromite catalyzing ultrafine AP: Evaluation of dispersity and mixing uniformity, *Defence Technology*, **32**: 120-133.
- P. R. Patil, V. N. Krishnamurthy, S. S. Joshi, (2008) Effect of nano-copper oxide and copper chromite on the thermal decomposition of ammonium perchlorate, *Propellants, Explosives, Pyrotechnics*, **33**: 266-270.
- M. A. Kassem, A. Abu El-Fadl, A. M. Nashaat, H. Nakamura, (2020) Magnetic evolution from the superparamagnetism in nanospinel chromites Cd_{1-x}CoxCr₂O₄ (0 ≤ x ≤ 1.0), *Journal of Magnetism and Magnetic Materials*, **495**: 165830.
- F. Paborji, M. Shafiee Afarani, A. M. Arabi, M. Ghahari, (2023) Solution combustion synthesis of FeCr₂O₄:Zn,Al pigment powders, *International Journal of Applied Ceramic Technology*, **20**: 2203-2216.
- V. T. Vader, (2017) Ni and Co substituted zinc ferri-chromite: A study of their influence in photocatalytic performance, *Materials Research Bulletin*, **85**: 18-22.
- M. Ahmadyari-Sharamin, S. A. Hassanzadeh-Tabrizi, (2021) Polyacrylamide gel synthesis, characterization, and optical properties of Co_{1-x}NixCr₂O₄ spinel nanopigment, *Journal of Sol-Gel Science and Technology*, **99**: 534-545.
- S. Naz, S. K. Durrani, M. Mehmood, M. Nadeem, A. A. Khan, (2016) Study of thermal, structural and impedance characteristics of nanocrystalline copper chromite synthesized via hydrothermal process, *Journal of Thermal Analysis and Calorimetry*, **126**: 381-389.
- P. S. Kumari, D. R. Kumar, G. V. Charan, S. R. Sagurthi, (2023) Structural, photocatalytic, and anticancer activity Ni-substituted Cu nanochromites synthesized by citrate gel auto-combustion method, *Chemical Papers*, **77**: 4727-4745.
- P. Sailaja Kumari, G. Vijaya Charan, D. Ravi Kumar, (2022) Synthesis, structural, photocatalytic and anti-cancer activity of Zn doped Ni nano chromites by citrate gel auto combustion method, *Inorganic Chemistry Communications*, **139**: 109393.
- Y. El Jabbar, H. Lakhli, R. El Ouatib, L. Er-Rakho, S. Guillemet-Fritsch, B. Durand, (2021) Green nanoceramic pigments based on cobalt chromite doped with Al: Synthesis, characterisation and colour performance, *Ceramics International*, **47**: 9373-9381.
- S. M. El-Sheikha, M. Rabbah, (2013) Novel low temperature synthesis of spinel nano-magnesium chromites from secondary resources, *Thermochimica Acta*, **568**: 13-19.
- S. Naz, S. K. Durrani, M. Mehmood, M. Nadeem, (2016) Hydrothermal synthesis, structural and impedance studies of nanocrystalline zinc chromite spinel oxide material, *Journal of Saudi Chemical Society*, **20**: 585-593.
- P. Mohanty, C. J. Sheppard, A. R. E. Prinsloo, W. D. Roos, L.



- Oliví, G. Aquilanti, (2018) Effect of cobalt substitution on the magnetic properties of nickel chromite, *Journal of Magnetism and Magnetic Materials*, **451**: 20-28.
19. X. Xu, J. Gao, W. Hong, (2016) Ni-based chromite spinel for high-performance supercapacitors, *RSC Advances*, **6**: 29646-29653.
 20. M. Saeed, M. Rani, K. Batool, H. Batool, A. Younus, S. Azam, A. Mehmood, B. Haq, T. Alshahrani, G. Ali, M. Maqbool, (2021) Synthesis and fabrication of $\text{Co}_{1-x}\text{Ni}_x\text{Cr}_2\text{O}_4$ chromate nanoparticles and the effect of Ni concentration on their Bandgap, structure, and optical properties, *Journal of Composites Science*, **5**: 247.
 21. S. A. Bakar, N. Soltani, W. M. M. Yunus, E. Saion, A. Bahrami, (2014) Structural and paramagnetic behavior of spinel NiCr_2O_4 nanoparticles synthesized by thermal treatment method: Effect of calcination temperature, *Solid State Communications*, **192**: 15-19.
 22. Y. Benrighi, N. Nasrallah, T. Chaabane, H. Belkacemi, K. W. Bourkeb, H. Kenfoud, O. Baaloudj, (2022) Characterization and application of the spinel CuCr_2O_4 synthesized by sol-gel method for sunset yellow photodegradation, *Journal of Sol-Gel Science and Technology*, **101**: 390-400.
 23. V. Mykhailovych, A. Kanak, S. Cojocaru, E. D. Chitoiu-Arsene, M. N. Palamaru, A. R. Iordan, O. Korovyanko, A. Diaconu, V. G. Ciobanu, G. Caruntu, O. Lushchak, P. Fochuk, Y. Khalavka, A. Rotaru, (2021) Structural, optical, and catalytic properties of MgCr_2O_4 spinel-type nanostructures synthesized by Sol-Gel auto-combustion method, *Catalysts*, **11**: 1476.
 24. S. Heni, S. Heini, M. L. Bouazizi, L. HajTaieb, A. Dhahri, H. Ben Bacha, (2024) Improving the optical properties of magnesium spinel chromites through Ni and Cu substitutions for optoelectronic applications, *RSC Advances*, **14**: 26340-26353.
 25. H. Dhibi, O. Rejaiba, J. Khelifi, M. Nasri, K. Khirouni, M. L. Bouazizi, E. K. Hlil, (2023) Comprehensive investigation of structural, morphologic, optical, dielectric and electrical of $\text{Ni}_0.3\text{Cd}_0.7\text{Cr}_2\text{O}_4$ chromite to optoelectronic application, *Journal of Inorganic and Organometallic Polymers and Materials*, **33**: 3984-4000.
 26. H. Dhibi, O. Rejaiba, J. Khelifi, M. Nasri, O. Amorri, K. Khirouni, M. L. Bouazizi, (2023) Detailed study of structural, optical, dielectric and electrical properties of $\text{Ni}_0.7\text{Cd}_0.3\text{Cr}_2\text{O}_4$ (NCCO) chromite prepared using sol-gel method, *Journal of Sol-Gel Science and Technology*, **108**: 159-174.
 27. D. Zhang, X. Zhang, Z. Zhang, X. Zhang, F. Qiu, Z. Liu, W. Li, (2022) Treatment of methylene blue wastewater with nano- PbCrO_4 photocatalyst prepared from chromite ore processing residue, *Journal of Cleaner Production*, **379**: 134352.
 28. K. Batool, M. Rani, A. Younus, A. Mehmood, S. Azam, B. U. Haq, R. Shafique, N. Akhtar, W. Khan, T. Alshahrani, (2020) Nanosized magnesium doped copper chromites spinel particles synthesis and characterization, *ECS Journal of Solid State Science and Technology*, **9**: 126005.
 29. S. Taghavi Fardood, R. Forootan, F. Moradnia, Z. Afshari, A. Ramazani, (2020) Green synthesis, characterization, and photocatalytic activity of cobalt chromite spinel nanoparticles, *Materials Research Express*, **7**: 015086.
 30. W. M. Gamal, A. A. H. El-Bassuony, H. K. Abdelsalam, (2024) Fascinating study of elastic, FTIR, and antimicrobial properties of silver nanochromite at different annealing temperatures, *Polymer Bulletin*, **81**: 1821-1837.
 31. A. Ajith, T. A. Wani, G. Suresh, N. Saravanan. (2024) A facile synthesis and characterization of spinel Zinc-Chromite (ZnCr_2O_4) nanoparticles: Their photocatalytic, antibacterial, and anticancer activities, *Journal of Sol-Gel Science and Technology*, **110**: 74-89.
 32. I. El Hajjar, M. Al Bitar, S. Zahr, R. Zahr, M. Khalil, R. Awad, (2023) Investigation of the physical properties and antibacterial activity of various ferrite, chromite, and aluminate nanocomposites, *Journal of Alloys and Compounds*, **968**: 171953.
 33. M. A. Sayed, T. M. A. A. El-Rahman, H. K. Abdelsalam, A. M. Ali, M. M. Hamdy, Y. A. Badr, N. H. A. E. Rahman, S. M. A. El-Latif, S. H. Mostafa, S. S. Mohamed, Z. M. Ali, A. A. H. El-Bassuony, (2022) Attractive study of the antimicrobial, antiviral, and cytotoxic activity of novel synthesized silver chromite nanocomposites, *BMC Chemistry*, **16**: 39.

*Bibliographical Sketch



Dr. G. Vijaya Charan is working as Professor at Department of Chemistry, University College of Science, Osmania University. She has completed her M.Sc. with Inorganic Chemistry specialization from University College for Women Koti, Osmania University, in 1999 and she was awarded Ph.D. from University College of Science, Osmania University, under the able guidance of Prof. B. Satyanarayana University College of Science, Osmania University, on the topic "Novel green Zirconia doped heterogeneous Metal Oxide Catalysts in various organic transformations". She has 25 years of teaching experience and 20 years of research experience. She has published 30 research publications in various National and International journals. She has completed two UGC research projects and one DST project. Currently seven research scholars are working under her supervision. She is also a member in the organizing committee to conduct the seminars, conferences and workshops. Her area of research work is Synthesis of Catalysts, Nano-materials and studying their Characterization and Applications. Evaluator for projects and seminars presented by students. She has attended and presented Papers, Posters at various National and International Seminars/Conferences/Workshops. Her Academic and Administrative achievements, as Academic Coordinator, Head of the Department, Student Advisor, and also a member for women's cell Committee.

